31. T. Apichattrabrut, K. Ravi-Chandar, *Mech. Adv. Mater. Structures* **13**, 61 (2006).
32. P. Fratzl, H. S. Gupta, F. D. Fisher, O. Kolednik, *Adv. Mater.* **19**, 2657 (2007).
33. H. Ming-Yuan, J. W. Hutchinson, *Int. J. Solids Struct.* **25**, 1053 (1989).
34. V. Imbeni *et al.*, *Nat. Mater.* **4**, 229 (2005).
35. K. S. Chan, M. Y. He, J. W. Hutchinson, *Mater. Sci. Eng. A* **167**, 57 (1993).
36. R. Wang, H. S. Gupta, *Annu. Rev. Mater. Res.* **41**, 41 (2011).
37. W. K. Brooks, *Report on the Scientific Results of the Exploring Voyage of the H.M.S. Challenger*, vol. 45, *Stomatopoda* (Neill and Co., Edinburgh, 1886).

REPORTS

Quantum Information Storage for over 180 s Using Donor Spins in a ^{28}Si "Semiconductor Vacuum"

M. Steger,[1] K. Saeedi,[1] M. L. W. Thewalt,[1]* J. J. L. Morton,[2] H. Riemann,[3] N. V. Abrosimov,[3] P. Becker,[4] H.-J. Pohl[5]

A quantum computer requires systems that are isolated from their environment, but can be integrated into devices, and whose states can be measured with high accuracy. Nuclear spins in solids promise long coherence lifetimes, but they are difficult to initialize into known states and to detect with high sensitivity. We show how the distinctive optical properties of enriched ^{28}Si enable the use of hyperfine-resolved optical transitions, as previously applied to great effect for isolated atoms and ions in vacuum. Together with efficient Auger photoionization, these resolved hyperfine transitions permit rapid nuclear hyperpolarization and electrical spin-readout. We combine these techniques to detect nuclear magnetic resonance from dilute ^{31}P in the purest available sample of ^{28}Si, at concentrations inaccessible to conventional measurements, measuring a solid-state coherence time of over 180 seconds.

I f computers could store and process quantum information, they could solve a host of problems that are intractable with even the fastest of modern supercomputers. Among the many different physical systems proposed to implement such a quantum computer (*1*), there is a trade-off between the low error rates and exquisite control exhibited by quantum systems in high-vacuum environments (*2*) versus the inherent scalability and device compatibility offered by solid-state systems (*3*). One promising solution is to identify suitable ultrapure materials offering a vacuumlike environment to quantum systems residing within. Motivated by its central role in conventional electronics, silicon has become one of the most highly purified materials, with impurity and defect densities typically measured in parts per billion or below. Even the isotopic variation in silicon (which exists as ^{28}Si, ^{29}Si, and ^{30}Si, with only ^{29}Si having nonzero nuclear spin) can be addressed, with 99.995% ^{28}Si material produced as part of a project to redefine the kilogram (*4*). Silicon therefore offers the potential to bridge the gap between these approaches to quantum information processing: providing

[1]Department of Physics, Simon Fraser University, Burnaby, BC V5A 1S6, Canada. [2]Department of Materials, Oxford University, Oxford OX1 3PH, UK. [3]Leibniz-Institut für Kristallzüchtung, 12489 Berlin, Germany. [4]PTB (Physikalisch-Technische Bundesanstalt) Braunschweig, 38116 Braunschweig, Germany. [5]Vitcon Projectconsult GmbH, 07745 Jena, Germany.

*To whom correspondence should be addressed. E-mail: thewalt@sfu.ca

Fig. 1. Spin-selective creation of the D^{0}X is used to polarize and read out the ^{31}P nuclear spin. (**A**) The ground states of the D^{0}X and D^0 and their splittings under a magnetic field, showing the origin of the 12 dipole-allowed absorption transitions, labeled from 1 to 12 in order of increasing energy (*E*). (**B**) The hyperpolarization mechanism used here polarizes D^0 into hyperfine state $|3\rangle$, with polarizing laser on line 6, readout laser on line 4, and RF applied at RF$_\uparrow$. The single and double arrows denote the electron and nuclear spins, respectively. (**C**) Photoconductivity spectra at T = 4.2 K and B = 845 G, for the largely unpolarized equilibrium case (bottom) and using the hyperpolarization scheme (top). The relative intensities of lines 3, 4, 9, and 10 give directly the relative populations of D^0 states $|3\rangle$, $|4\rangle$, $|1\rangle$, and $|2\rangle$, respectively.
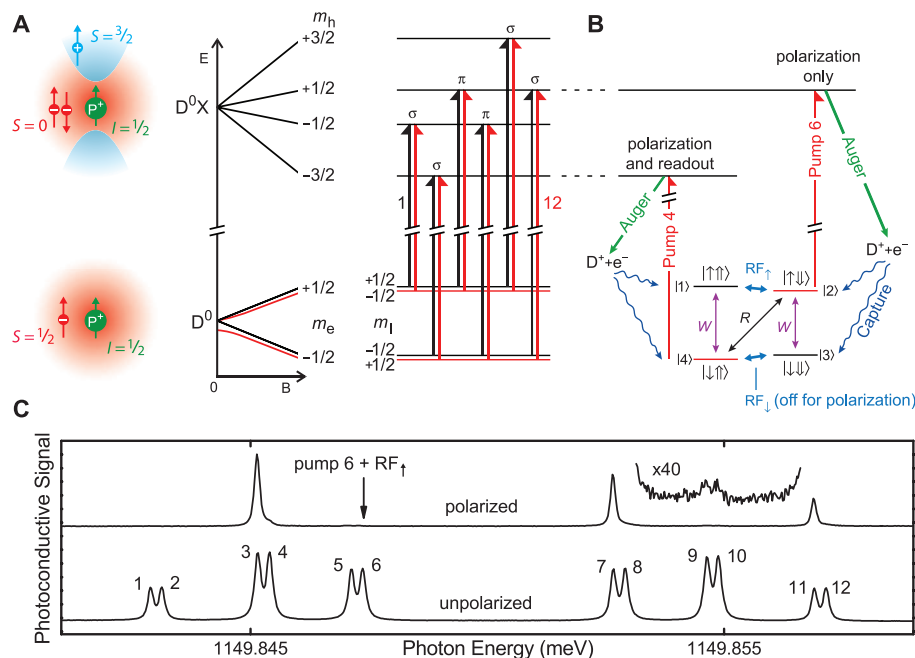
long quantum information lifetimes and high-fidelity operations within a semiconductor device.

The coherence time (T_2) of quantum information is a fundamental metric in comparing diverse physical quantum bit (qubit) candidates; indeed, it is the time scale on which a quantum bit turns into a classical one (5). In a seminal proposal by Kane (6), the nuclear spin of neutral donor impurities (D^0) in silicon was identified as a promising qubit candidate because of its long T_2, as well as the possibility of control and readout via its hyperfine coupling to the D^0 electron spin. A resurgence of interest in donors in Si ensued, bringing new schemes for preparing, coupling, and measuring their electron and nuclear spins (7–20). The storage and retrieval of either quantum (7) or classical (8) information between the donor electron and nuclear spins, and the entanglement of these spins (9), have been demonstrated.

For phosphorus, the prototypical donor in ^{28}Si, the reported electron T_2 (T_{2e}) is found to be inversely proportional to the donor density (for densities in the range from 10^{14} to 10^{16} cm^{-3}), and a similar observation has been made for the nuclear T_2 (T_{2n}) (10). This motivates the study of coherence lifetimes at even lower donor densities; however, densities of 10^{13} cm^{-3} are at the limit of detection by conventional electron spin resonance and electron nuclear double-resonance (ENDOR) and orders of magnitude below that of standard nuclear magnetic resonance (NMR). We show that isotopically enriched ^{28}Si not only provides a nuclear-spin-free environment, which leads to long T_{2e} and T_{2n} (7, 10, 15), but also permits a method for spin polarization and detection,

which opens the door to exploring magnetic resonance of donors at densities below 10^{12} cm^{-3}. The resulting coherence times exceed those of other solid-state systems (21) and are comparable to the longest measured for isolated atoms and ions in vacuum (22).

The elimination of the 4.6% of ^{29}Si (with nuclear-spin quantum number $I = 1/2$) present in natural Si removes a primary decoherence mechanism for the donor electron spin (10). However, enriched ^{28}Si has another crucial advantage resulting simply from the mass differences between the three stable isotopes. In ^{28}Si, a variety of long-studied optical transitions are much sharper and better resolved, often by over an order of magnitude, than in natural Si because of the unanticipated dominant inhomogeneous broadening as a result of the mixed host isotopes (16–19). In particular, the ability to resolve the hyperfine splitting of the D^0 ground state in the transitions between D^0 and the neutral donor-bound exciton (D^0X) in ^{28}Si lies at the heart of our spin polarization and detection methods. ^{28}Si can be thought of as a "semiconductor vacuum," with properties almost identical to those of Si, but with almost no nuclear spins, and optical line-widths approaching their homogeneous, lifetime-limited values (23).

D^0X in indirect-gap semiconductors such as Si have a property that is usually considered disadvantageous but that is central to our new methods. The indirect band gap results in long radiative lifetimes, and D^0X recombination is dominated by nonradiative Auger decay, in which D^0X decay to ionized donors (D^+) and energetic

free electrons (24). This results in very low luminescence quantum efficiencies, ~10^{-4} for the phosphorus D^0X, limiting the use of luminescence to monitor the D^0X population as done in our previous studies (17–19). However, we can instead detect the electrons produced with ~100% efficiency by Auger decay to monitor the resonant creation of D^0X in a version of optically detected magnetic resonance that we refer to as Auger-electron-detected magnetic resonance (AEDMR).

The sample used in this study is enriched to 99.995% ^{28}Si and contains 5×10^{11} cm^{-3} of ^{31}P and 5×10^{13} cm^{-3} of the acceptor boron, making it p-type (25). In a p-type sample in equilibrium at cryogenic temperature, one expects all the donors to be D^+ and an equal number of acceptors to also be ionized (A^-), making resonant D^0X creation impossible. Weak above-gap radiation, here supplied by a 1047-nm laser, generates a sufficient concentration of electrons and holes to photoneutralize the D^- and A^+ (25).

The phosphorus D^0 and D^0X states and optical transitions are outlined in Fig. 1, along with optical spectra demonstrating the hyperpolarization results. A schematic of the D^0 and D^0X ground states, together with their Zeeman splittings for the case of $B \parallel [001]$, includes the hyperfine splitting of the D^0 ground state resulting from the $I = 1/2$ nuclear spin but ignores the negligible nuclear Zeeman energy in the D^0X states (the bare nuclear Zeeman energies are small at these low fields, and the contact hyperfine interaction with the D^0X hole is vanishingly small) (Fig. 1A). The 12 dipole-allowed transitions

Fig. 2. NMR of ^{31}P in ^{28}Si using AEDMR. (**A**) Pulse sequence for a Hahn echo measurement. The 500-ms polarizing stage hyperpolarizes the system into state $|3\rangle$, with magnetization in the $+\mathbf{Z}$ direction. The NMR manipulation occurs in the dark and begins with a $\pi/2$ preparation pulse, which rotates the initial polarization into the $\mathbf{XY}$ plane. After the τ-π-τ Hahn refocusing sequence, a second $\pi/2$ pulse projects the remaining coherent magnetization back into the $\mathbf{Z}$ direction for readout. The 1047-nm laser and then the readout laser are turned on, generating a photoconductive transient with area proportional to the population in $|4\rangle$. A π pulse then swaps the $|4\rangle$ and $|3\rangle$ populations, producing a second photoconductive transient proportional to the population previously in $|3\rangle$. (**B**) Single-shot photoconductive readout transients for the system polarized into either states $|3\rangle$ or $|4\rangle$ or unpolarized. (**C**) Single-shot measurements of the Hahn echo decay at $T = 1.74$ K, with an exponential fit.
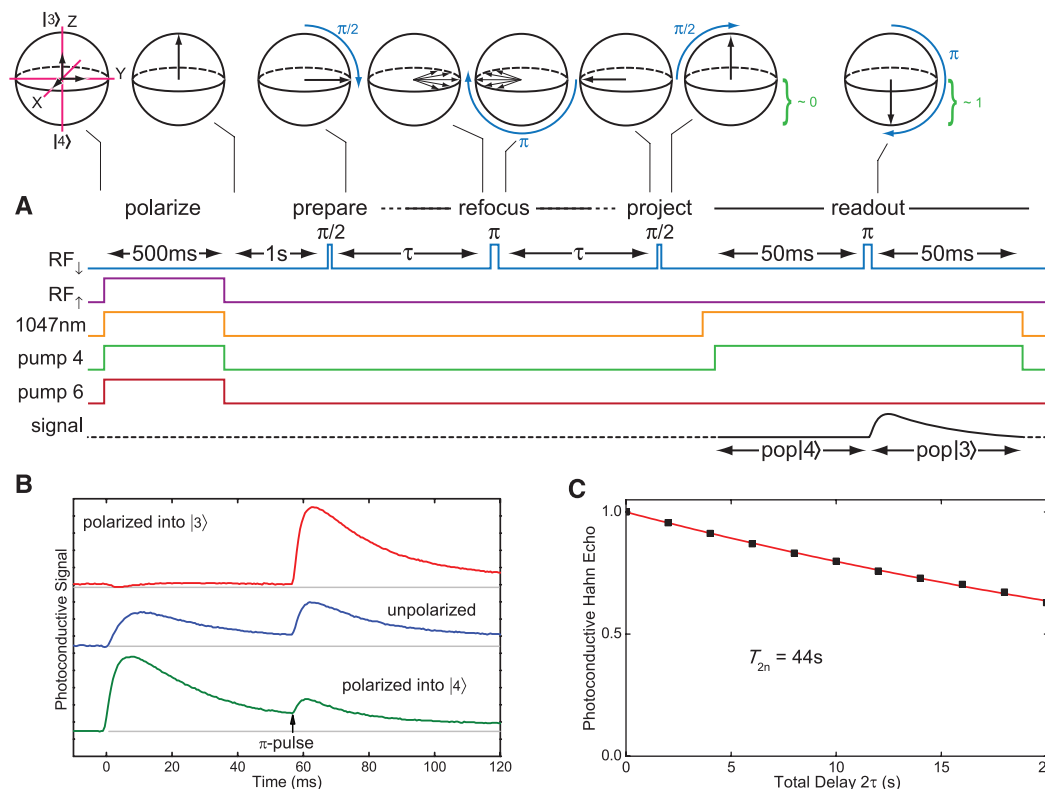
between the four D^0 hyperfine states and the four D^0X states are labeled from 1 to 12 in order of increasing energy. Figure 1B shows the D^0 state labels used here, and the hyperpolarization scheme for the specific case of a high-power polarizing laser on line 6, which has the effect of pumping D^0 from state $|2\rangle$ to state $|3\rangle$ (the D^0X ionizes with near-unity probability, and some of the thermalized electrons are recaptured with opposite spin into $|3\rangle$). We simultaneously applied an NMR field $RF_\uparrow$, such that D^0 in $|1\rangle$ were pumped to $|2\rangle$, as well as a low-power "readout" laser tuned to line 4, pumping population from $|4\rangle$ to $|1\rangle$ (this could also be achieved by applying a microwave field at the $|4\rangle \leftrightarrow |1\rangle$ energy). The result is that the D^0 population is pumped into state $|3\rangle$, where both electron and nuclear spin are in the spin-down state. The results were measured by a noncontact photoconductive detection method as the readout laser was scanned across the 12 D^0X transitions (low-power above-gap excitation is present in all cases) (Fig. 1C). From the relative intensities in Fig. 1C, we find that 94% of D^0 are pumped to $|3\rangle$, resulting in a net electron polarization $P_e = 0.97$ and nuclear polarization $P_n = 0.90$. At this magnetic field and temperature, the electron equilibrium spin polarization is 0.014, so the hyperpolarization enhancement is 69; the nuclear equilibrium spin polarization is 4×10^{-5}, and the hyperpolarization enhancement is 22,000. This nuclear polarization, which occurs with a time constant of 100 ms or less, is faster and more effective than previous schemes for impurities in a semiconductor (7, 11, 19).

We combined hyperpolarization, coherent manipulation of the nuclear spin, and readout by AEDMR to make measurements of T_{2n}. Figure 2A shows the optical and RF pulse sequence for a Hahn echo measurement. During the polarization stage, we prepared state $|3\rangle$. Two $RF_\downarrow$ pulses were applied to implement the Hahn echo sequence, with a final $\pi/2$ $RF_\downarrow$ pulse for readout. All RF pulses are of the same phase (nominally X). If the nuclear spin has remained coherent, all population is returned to state $|3\rangle$; otherwise it becomes equally (and incoherently) distributed between states $|3\rangle$ and $|4\rangle$. The readout stage therefore measures the difference between the areas of the $|3\rangle$ and $|4\rangle$ photoconductive transients (Fig. 2B). By varying the delay τ in the Hahn echo sequence, we obtain a T_{2n} of 44 s at $T = 1.74$ K (Fig. 2C).

Just as the Hahn echo sequence removes the effects of a static distribution of precession frequencies, dynamic decoupling, through a periodic reversal of the spins' interaction with the environment, can mitigate the effects of environmental fluctuations on a time scale slower than this period (26, 27). The simplest of these that can maintain an arbitrary initial state are periodic sequences of $\pm\pi$ rotations about the orthogonal X and Y axes, with equal delays (2τ) between all π pulses. Our best results were obtained by using the XY-16 sequence (28), re-

sulting in the single-shot coherence decays as a function of sample temperature (Fig. 3). Because $T_{2n} \leq 2T_{1e}$ (7), the $T_{2n} = 41$ s at 4.2 K is limited by T_{1e}, which we measure to be ~22 s, in good agreement with earlier studies (29). Below 4.2 K, T_{1e} rapidly becomes very long (29), and the observed T_{2n} must be limited by other processes, such as the residual ^{29}Si, or P-P dipolar coupling. Nevertheless, the observed T_{2n} becomes as long as 192 s at 1.74 K.

Lastly, we confirmed (Fig. 4) that the XY-16 sequence protects arbitrary initial states. The decay of X and Y initial states is seen to be essentially identical. The slower decay of the Z initial state reflects the fact that it is an eigenstate, not a coherent superposition, so it should decay as T_{1n}, not T_{2n}. At this temperature, T_{1n} is many hours, so the observed decay likely results from pulse errors in our XY-16 sequence (the 112-s delay corresponds to 1120 π pulses), although

Fig. 3. Coherence decays at several temperatures using the **XY**-16 periodic decoupling sequence. The single π pulse of the τ-π-τ refocusing sequence shown in Fig. 2 is replaced by a periodic sequence of rotations by $\pm\pi$ around the X or Y axes as indicated by the sequence at the top, with a delay of 2τ between all π pulses, where $\tau = 50$ ms for these measurements. Also shown are fits to exponential decays.
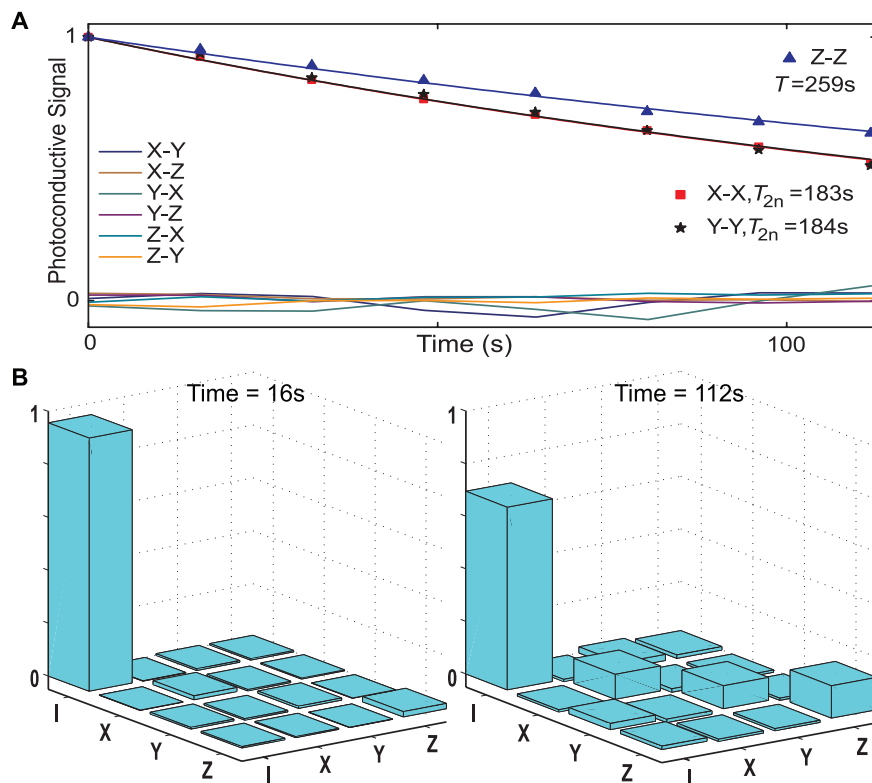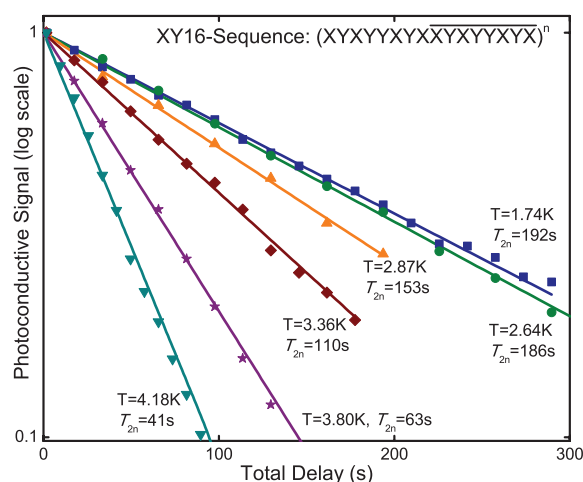

Fig. 4. Evaluating the performance of **XY**-16 dynamical decoupling. (**A**) α and β label the coherent magnetization after preparing the system in state α, dynamically decoupling for some time, and then measuring in the basis of β. The variations in the $\alpha \neq \beta$ data are indicative of the single-shot noise level, not cross-coupling resulting from the **XY**-16 sequence. (**B**) Quantum process tomography plots of the **XY**-16 sequence are shown for 16 and 112 s (25). $T = 2.64$ K and $\tau = 50$ ms.

some loss of D^0 because of ionization is also possible. By using these results, we can extract the quantum process tomography (25) of the sequence, confirming the close resemblance to the identity operator.

The AEDMR mechanism we introduce here should be extensible to the readout of single ^{31}P impurities (17, 30) and could be combined with the already demonstrated spin-dependent–tunneling electron spin readout of single ^{31}P (14). The method can be applied to other substitutional donors when ^{28}Si samples become available, and in particular Bi, where the much larger hyperfine coupling makes the hyperfine D^0X structure almost resolvable even in natural Si (20). The present p-type sample, together with our optical methods, would also be suited well to explore the NMR of ionized ^{31}P (D^+), which has recently been observed by using electrically detected ENDOR in natural Si (13) and should have very long T_{2n} in ^{28}Si. Such results would be important for the proposed cluster-state quantum computing scheme where quantum information is stored in the nuclear spins of ionized donors (31).

By eliminating almost all inhomogeneous broadening and host spins, highly enriched ^{28}Si approaches a semiconductor vacuum, enabling the use of hyperfine-resolved optical transitions, as is standard for atom and ion qubits in vacuum, but retaining the advantages of Si device technology, Auger photoionization for polarization and readout, and the ability to precisely and permanently place the qubit atoms (32).

References and Notes
1. D. Deutsch, *Proc. R. Soc. London Ser. A* **400**, 97 (1985).
2. J. P. Home et al., *Science* **325**, 1227 (2009); 10.1126/science.1177077.
3. J. J. L. Morton, D. R. McCamey, M. A. Eriksson, S. A. Lyon, *Nature* **479**, 345 (2011).
4. P. Becker, H.-J. Pohl, H. Riemann, N. V. Abrosimov, *Phys. Status Solidi A* **207**, 49 (2010).
5. T. D. Ladd et al., *Nature* **464**, 45 (2010).
6. B. E. Kane, *Nature* **393**, 133 (1998).
7. J. J. L. Morton et al., *Nature* **455**, 1085 (2008).
8. D. R. McCamey, J. Van Tol, G. W. Morley, C. Boehme, *Science* **330**, 1652 (2010).
9. S. Simmons et al., *Nature* **470**, 69 (2011).
10. A. M. Tyryshkin et al., *Nat. Mater.* **11**, 143 (2012).
11. D. R. McCamey, J. van Tol, G. W. Morley, C. Boehme, *Phys. Rev. Lett.* **102**, 027601 (2009).
12. H. Morishita et al., *Phys. Rev. B* **80**, 205206 (2009).
13. L. Dreher, F. Hoehne, M. Stutzmann, M. S. Brandt, *Phys. Rev. Lett.* **108**, 027602 (2012).
14. A. Morello et al., *Nature* **467**, 687 (2010).
15. W. M. Witzel, M. S. Carroll, A. Morello, Ł. Cywiński, S. Das Sarma, *Phys. Rev. Lett.* **105**, 187602 (2010).
16. M. Cardona, M. L. W. Thewalt, *Rev. Mod. Phys.* **77**, 1173 (2005).
17. A. Yang et al., *Phys. Rev. Lett.* **97**, 227401 (2006).
18. A. Yang et al., *Phys. Rev. Lett.* **102**, 257401 (2009).
19. M. Steger et al., *J. Appl. Phys.* **109**, 102411 (2011).
20. T. Sekiguchi et al., *Phys. Rev. Lett.* **104**, 137402 (2010).
21. T. D. Ladd, D. Maryenko, Y. Yamamoto, E. Abe, K. M. Itoh, *Phys. Rev. B* **71**, 014401 (2005).
22. C. Langer et al., *Phys. Rev. Lett.* **95**, 060502 (2005).
23. A. Yang et al., *Appl. Phys. Lett.* **95**, 122113 (2009).
24. W. Schmid, *Phys. Status Solidi B* **84**, 529 (1977).
25. Materials and methods are available as supplementary materials on *Science* Online.
26. L. Viola, S. Lloyd, *Phys. Rev. A* **58**, 2733 (1998).
27. A. M. Tyryshkin et al., http://arxiv.org/abs/:1011.1903v2 (2010).
28. T. Gullion, D. B. Baker, M. S. Conradi, *J. Magn. Reson.* **89**, 479 (1990).
29. G. Feher, E. A. Gere, *Phys. Rev.* **114**, 1245 (1959).
30. D. Sleiter et al., *New J. Phys.* **12**, 093028 (2010).
31. J. J. L. Morton, http://arxiv.org/abs/0905.4008v1 (2009).
32. S. R. Schofield et al., *Phys. Rev. Lett.* **91**, 136104 (2003).

Room-Temperature Quantum Bit Memory Exceeding One Second

P. C. Maurer,[1]* G. Kucsko,[1]* C. Latta,[1] L. Jiang,[2] N. Y. Yao,[1] S. D. Bennett,[1] F. Pastawski,[3] D. Hunger,[3] N. Chisholm,[4] M. Markham,[5] D. J. Twitchen,[5] J. I. Cirac,[3] M. D. Lukin[1]†

Stable quantum bits, capable both of storing quantum information for macroscopic time scales and of integration inside small portable devices, are an essential building block for an array of potential applications. We demonstrate high-fidelity control of a solid-state qubit, which preserves its polarization for several minutes and features coherence lifetimes exceeding 1 second at room temperature. The qubit consists of a single ^{13}C nuclear spin in the vicinity of a nitrogen-vacancy color center within an isotopically purified diamond crystal. The long qubit memory time was achieved via a technique involving dissipative decoupling of the single nuclear spin from its local environment. The versatility, robustness, and potential scalability of this system may allow for new applications in quantum information science.

M any applications in quantum communication (1) and quantum computation (2) rely on the ability to maintain qubit coherence for extended periods of time. Furthermore, integrating such quantum-mechanical systems in compact mobile devices remains an outstanding experimental task. Although trapped ions and atoms (3) can exhibit coherence times as long as minutes, they typically require a complex infrastructure involving laser cooling and ultrahigh vacuum. Other systems, most notably ensembles of electronic and nuclear spins, have also achieved long coherence times in bulk electron spin resonance (ESR) and nuclear magnetic resonance (NMR) experiments (4–6); however, owing to their exceptional isolation, individual preparation, addressing, and high-fidelity measurement remain challenging, even at cryogenic temperatures (7).

Our approach is based on an individual nuclear spin in a room-temperature solid. A nearby electronic spin is used to initialize the nuclear spin (8–10) in a well-defined state and to read it out in a single shot (10) with high fidelity. A combination of laser illumination and radio-frequency (rf) decoupling pulse sequences (4, 11) enables the extension of our qubit memory lifetime by nearly three orders of magnitude. This approach decouples the nuclear qubit from both the nearby electronic spin and other nuclear spins, demonstrating that dissipative decoupling can be a robust and effective tool for protecting coherence in various quantum information systems (2, 12, 13).

Our experiments used an individual nitrogen-vacancy (NV) center and a single ^{13}C ($I = 1/2$) nuclear spin (Fig. 1A) in a diamond crystal. We worked with an isotopically pure diamond sample, grown using chemical vapor deposition from isotopically enriched carbon consisting of 99.99% spinless ^{12}C isotope. In such a sample, the optically detected ESR associated with a single NV center is only weakly perturbed by ^{13}C nuclear spins, resulting in long electronic spin coherence times (14). This allows us to make use of a Ramsey pulse sequence to detect a weakly coupled single nuclear spin, separated from the NV by 1 to 2 nm. The coupling strength at such a distance is sufficiently large to enable preparation and measurement of the nuclear-spin qubit with high fidelity. For the concentration of ^{13}C nuclei we used, about 10% of all NV centers exhibited a coupled nuclear spin with a separation of this order.

In our experimental setup, the diamond sample was magnetically shielded from external perturbations, and a static magnetic field $B = 244.42 \pm 0.02$ G was applied along the NV symmetry axis.

[1]Department of Physics, Harvard University, Cambridge, MA 02138, USA. [2]Institute for Quantum Information and Matter, California Institute of Technology, Pasadena, CA 91125, USA. [3]Max-Planck-Institut für Quantenoptik, Garching D-85748, Germany. [4]School of Engineering and Applied Sciences, Harvard University, Cambridge, MA 02138, USA. [5]Element Six, Ascot SL5 8BP, UK.

*These authors contributed equally to this work.
†To whom correspondence should be addressed. E-mail: lukin@physics.harvard.edu